J Fluoresc (2013) 23:1139–1145
DOI 10.1007/s10895-013-1242-6

ORIGINAL PAPER

# A Pyrene-based Highly Selective Turn-on Fluorescent Chemosensor for Iron(III) Ions and its Application in Living Cell Imaging

**Peter Kun Chung · Shi-Rong Liu · Hsuan-Fu Wang · Shu-Pao Wu**

Received: 5 March 2013 / Accepted: 22 May 2013 / Published online: 4 July 2013


**Abstract** A new pyrene-based chemosensor (**1**) exhibits excellent selectivity for $Fe^{3+}$ ions over a wide range of tested metal ions $Ag^{+}$, $Ca^{2+}$, $Cd^{2+}$, $Co^{2+}$, $Cu^{2+}$, $Fe^{2+}$, $Hg^{2+}$, $K^{+}$, $Mg^{2+}$, $Mn^{2+}$, $Ni^{2+}$, $Pb^{2+}$, and $Zn^{2+}$. The binding of $Fe^{3+}$ to chemosensor **1** produces an emission band at 507 nm due to the formation of a Py-Py* excimer that is induced by $Fe^{3+}$-binding. The binding ratio of **1**-$Fe^{3+}$ was determined to be 1:1 from a Job plot. The association constant of **1**-$Fe^{3+}$ complexes was found to be $1.27\times10^{4}$ $M^{-1}$ from a Benesi-Hildebrand plot. In addition, fluorescence microscopy experiments show that **1** can be used as a fluorescent probe for detecting $Fe^{3+}$ in living cells.

**Keywords** Sensors · Iron · Pyrene · Imaging agents

## Introduction

Iron is the most abundant essential transition metal ion in the human body. Many proteins use iron as a cofactor in a wide range of biochemical processes, such as electron transport, oxygen transport, and oxidoreductase catalysis [1]. Iron distribution in the human body is a highly controlled process. A deficiency in iron reduces oxygen delivery to cells, resulting in exhaustion, poor work performance, and decreased immunity [2]. Conversely, iron overload in a living cell can lead to generation of reactive oxygen species (ROS) via the Fenton reaction, which can cause damage to lipids, nucleic acids, and proteins. The cellular toxicity of iron ions has been connected with serious diseases, including Alzheimer's, Huntington's, and Parkinson's disease [3–5].

P. K. Chung · S.-R. Liu · H.-F. Wang · S.-P. Wu (✉)
Department of Applied Chemistry, National Chiao Tung University, Hsinchu, Taiwan 300, Republic of China
e-mail: spwu@mail.nctu.edu.tw

Several methods for the detection of iron ions in various samples have been developed including atomic absorption spectrometry [6], inductively coupled plasma mass spectroscopy (ICPMS) [7], inductively coupled plasma-atomic emission spectrometry (ICP-AES) [8], and voltammetry [9]. These methods either require the destruction of the sample or are not suitable for on-site assays. Recently, more attention has been focused on the development of selective and sensitive fluorescent sensors for iron detection [10–20].

Because of the paramagnetic nature of $Fe^{3+}$, most reported fluorescent $Fe^{3+}$ chemosensors are based on a fluorescence quenching mechanism [21–25]. The design of "off-on" fluorescent $Fe^{3+}$ chemosensors remains a challenging task. In this study, a pyrene-based fluorescent chemosensor was designed for metal ion detection. Chemosensor **1** was synthesized through the reaction of 1-pyrenecarboxaldehyde hydrazone and 1,4-bis(2-formylphenoxy)butane to form two imine bonds between 1,4-bis-phenoxybutane and pyrene (Scheme 1). Chemosensor **1** exhibits weak fluorescence due to fluorescence quenching by photoinduced electron transfer from the electrons on the nitrogen atom to pyrene. Binding metal ions to the chemosensor induces the formation of a Py-Py* excimer. The metal ions $Ag^{+}$, $Ca^{2+}$, $Cd^{2+}$, $Co^{2+}$, $Cu^{2+}$, $Fe^{2+}$, $Fe^{3+}$, $Hg^{2+}$, $K^{+}$, $Mg^{2+}$, $Mn^{2+}$, $Ni^{2+}$, $Pb^{2+}$, and $Zn^{2+}$ were tested for metal ion binding selectivity with chemosensor **1**, but $Fe^{3+}$ was the only ion that caused a visible color change (from colorless to yellow) and a green emission upon binding with chemosensor **1**.

## Experiment Section

### Materials and Instrumentations

All reagents were obtained from commercial sources and used as received without further purification. UV/Vis spectra were

**Scheme 1** Synthesis of chemosensor **1**

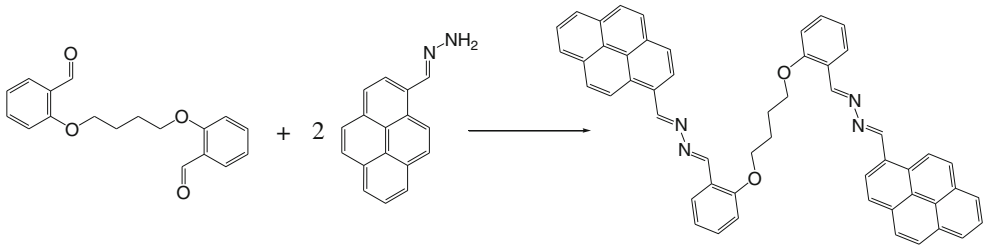

recoreded on an Agilent 8453 UV/Vis spectrometer. IR data were obtained on Bomem DA8.3 Fourier-Transform Infrared Spectrometer. NMR spectra were obtained on a Bruker DRX-300 NMR spectrometer. Fluorescence imagings were obtained on a ZEISS Axio Scope A1 Fluorescence Microscope.

## Synthesis of Chemosensor 1

To a solution containing 1-pyrenecarboxaldehyde hydrazone [26] (0.122 g, 0.5 mmol) in methanol (50 mL), 1,4-bis (2-formylphenoxy)butane [27] (0.0775 g, 0.26 mmol) was added and the mixture was then heated at 80 °C for 4 h. The resulting yellow precipitate was filtered and washed with methanol (30 mL×3). The product was recrystallized by $CH_2Cl_2$/hexane (1:10, v/v) to give a compound **1** as a yellow solid. Yields: 114.5 mg (61 %); m.p. 229–230 °C.$^1$H-NMR (600 MHz, $CDCl_3$): δ 9.57 (s, 2H), 9.24 (s, 2H), 8.72 (d, J=9.4 Hz, 2H), 8.59 (d, J=8.2 Hz, 2H), 7.91–8.16 (m, 16H), 7.36 (t, J=7.6 Hz, 2H), 6.97 (m, 4H), 4.17 (s, 4H), 2.12 (s, 4H).$^{13}$C-NMR (150 MHz, $CDCl_3$): δ 160.2, 158.7, 157.92, 133.3, 132.6, 131.3, 130.7, 130.4, 128.7, 128.7, 127.6, 127.4, 127.0, 126.3, 126.1, 125.9, 125.8, 124.9, 124.7, 123.2, 122.8, 121.0, 112.3, 68.3, 26.3. IR ($cm^{-1}$): 3042.3, 2938.1, 2873.5, 1613.2, 1458, 1249.7. MS(ESI): 751.6. HRMS(ESI): calcd. for $C_{52}H_{39}N_4O_2$: 751.3073; found 751.3073.

## Metal ion Binding Study by UV–vis and Fluorescence Spectroscopy

Chemosensor **1** (2 μM) was added with different metal ions (20 μM). All spectra were measured in 1.0 mL acetonitrile-acetone solution (v/v=99:1). The light path length of cuvette was 1.0 cm.

## Determination of the Binding Stochiometry and the Association Constants $K_a$ of Cu(II) Binding in Chemosensor 1

The binding stochiometry of **1**-$Fe^{3+}$ complexes was determined by Job plot experiments. The fluorescence intensity at 507 nm was plotted against molar fraction of **1** under a constant total concentration (10 μM). The concentration of the complex approached a maximum intensity when the molar fraction was 0.5 [28]. These results indicate that chemosensor **1** forms a 1:1 complex with $Fe^{3+}$. The apparent association constants ($K_a$) of **1**-$Fe^{3+}$ complexes was determined by the Benesi-Hildebrand Eq. 1 [29, 30]:

$$1/(F-F_0) = 1/\{K_a * (F_{max}-F_0) * [Fe^{3+}]\} + 1/(F_{max}-F_0), \quad (1)$$

where $F$ is the fluorescence intensity at 507 nm at any given $Fe^{3+}$ concentration, $F_0$ is the fluorescence intensity at 507 nm in the absence of $Fe^{3+}$, and $F_{max}$ is the maxima fluorescence intensity at 507 nm in the presence of $Fe^{3+}$ in solution. The association constant $K_a$ was evaluated graphically by plotting $1/(F–F_0)$ against $1/[Fe^{3+}]$. Typical plots ($1/(F–F_0)$ vs. $1/[Fe^{3+}]$) are shown in Fig. 4. Data were linearly fitted according to Eq. (1) and the $K_a$ value was obtained from the slope and intercept of the line.

## Cell Culture

The cell line HeLa was provided by the Food Industry Research and Development Institute (Taiwan). The HeLa cells were grown in DMEM (Dulbecco's modified Eagle's medium) supplemented with 10 % FBS (fetal bovine serum) at 37 °C and 5 % $CO_2$. Cells were plated on 14 mm glass coverslips and allowed to adhere for 24 h.

## Fluorescence Imaging

Experiments to assess the $Fe^{3+}$ uptake were performed in phosphate-buffered saline (PBS) with 20 μM $FeCl_3$. The cells cultured in DMEM were treated with 10 mM solutions of $FeCl_3$ (2 μL; final concentration: 20 μM) dissolved in sterilized PBS (pH=7.4) and incubated at 37 °C for 30 min. The treated cells were washed with PBS (3×2 mL) to remove remaining metal ions. DMEM (2 mL) was added to the cell culture, which was then treated with a 10 mM solution of chemosensor **1** (2 μL; final concentration: 20 μM) dissolved in DMSO. The samples were incubated at 37 °C for 30 min. The culture medium was removed, and the treated cells were washed with PBS (3× 2 mL) before observation. Fluorescence imaging was performed with a ZEISS Axio Scope A1 fluorescence microscope. Cells loaded with chemosensor **1** were excited at 480 nm by using a 50 W Hg lamp.

## Quantum Chemical Calculation

Quantum chemical calculations based on density functional theory (DFT) were carried out using a Gaussian 09 program.

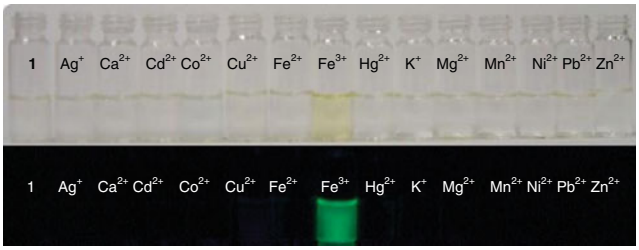


**Fig. 1** Color (*top*) and fluorescence (*bottom*) changes of chemosensor **1** (2 μM) upon addition of various metal ions (20 μM) in acetonitrile-acetone (v/v=99:1) solutions

Optimized geometry of **1**-$Fe^{3+}$ complex was performed using the B3LYP functional and the LANL2DZ basis set.

## Results and Discussion

### Synthesis of Chemosensor 1

Chemosensor **1** was synthesized through the reaction of 1-pyrenecarboxaldehyde hydrazone and 1,4-bis(2-formylphenoxy)butane to form two imine bonds between 1,4-bis-phenoxybutane and pyrene (Scheme 1). Chemosensor **1** is pale yellow and has an absorption band centered at 382 nm, which is a 47-nm red shift from the typical absorption band of pyrene, 335 nm [31]. Compared to the structure of pyrene, chemosensor **1** has longer conjugated double bonds. These are the reasons behind chemosensor **1** having a longer UV–vis absorption wavelength than pyrene. In addition, chemosensor **1** exhibits weak fluorescence (Φ=0.001) compared to pyrene (Φ=0.6~0.9) [32]. This is due to fluorescence quenching by photoinduced electron transfer from the electrons on the nitrogen atom to pyrene.

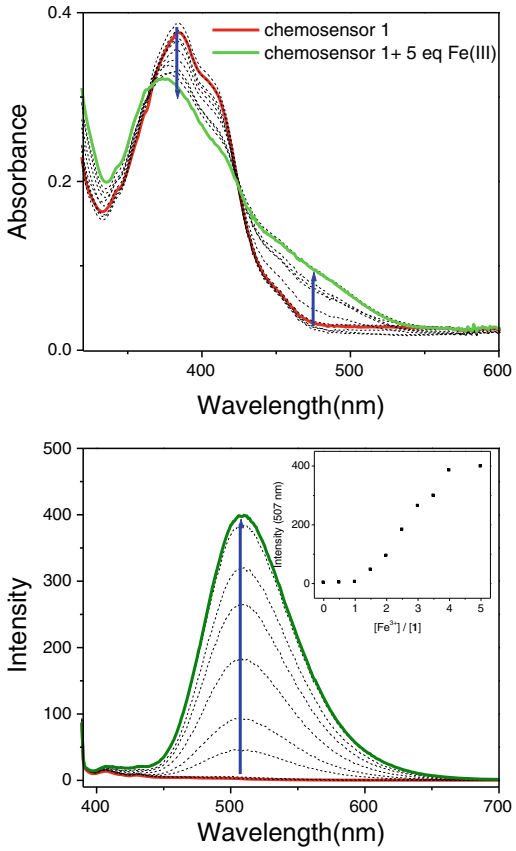


**Fig. 2** Absorption changes (*top*) and fluorescence response (*bottom*) of chemosensor **1** (4 μM) to various equivalents of $Fe^{3+}$ in $CH_3CN$/acetone (v/v=99:1) solutions. The excitation wavelength was 382 nm

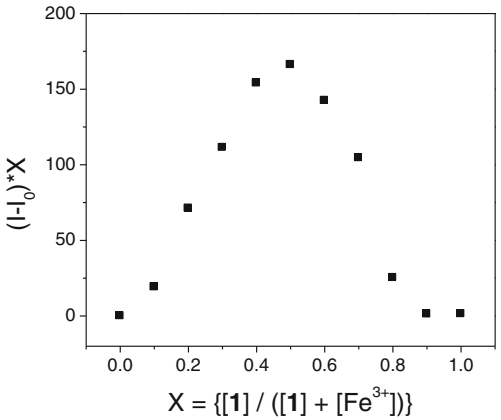


**Fig. 3** Job plot of the $Fe^{3+}$-**1** complexes in an acetonitrile-acetone (v/v=99:1) solution. The monitored emission wavelength was 507 nm. The total concentration of [**1**] and [$Fe^{3+}$] was 10 μM

### Cation-Sensing Properties

The sensing ability of chemosensor **1** was tested by mixing it with the metal ions $Ag^{+}$, $Ca^{2+}$, $Cd^{2+}$, $Co^{2+}$, $Cu^{2+}$, $Fe^{2+}$,

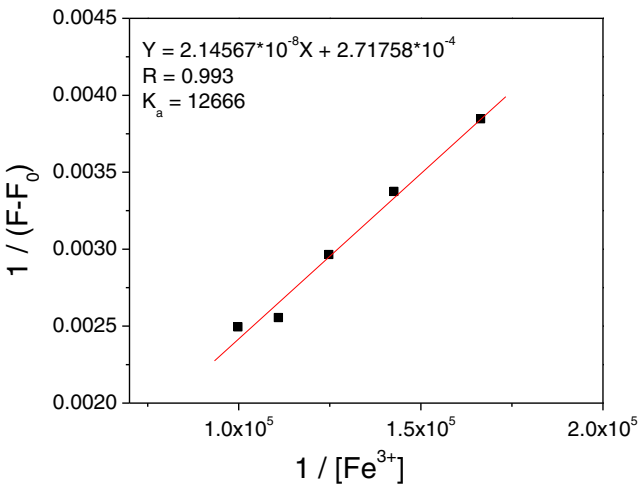


**Fig. 4** Benesi-Hildebrand plot of the $Fe^{3+}$-**1** complexes in acetonitrile-acetone (v/v=99:1) solutions

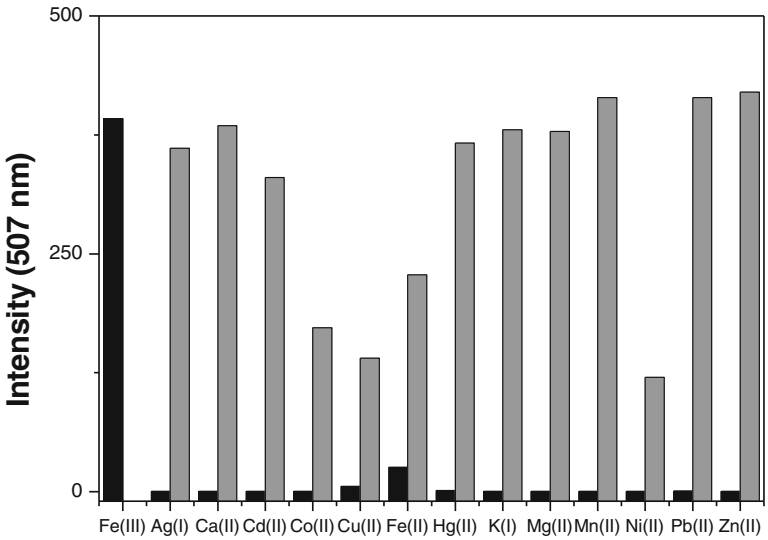


**Fig. 5** Fluorescence response of chemosensor **1** (2 μM) to $Fe^{3+}$ (10 μM) or 10 μM of other metal ions (the black bar portion) and to the mixture of other metal ions (10 μM) with 10 μM of $Fe^{3+}$ (the gray bar portion) in acetonitrile-acetone (v/v=99:1) solutions. The excitation wavelength was 382 nm

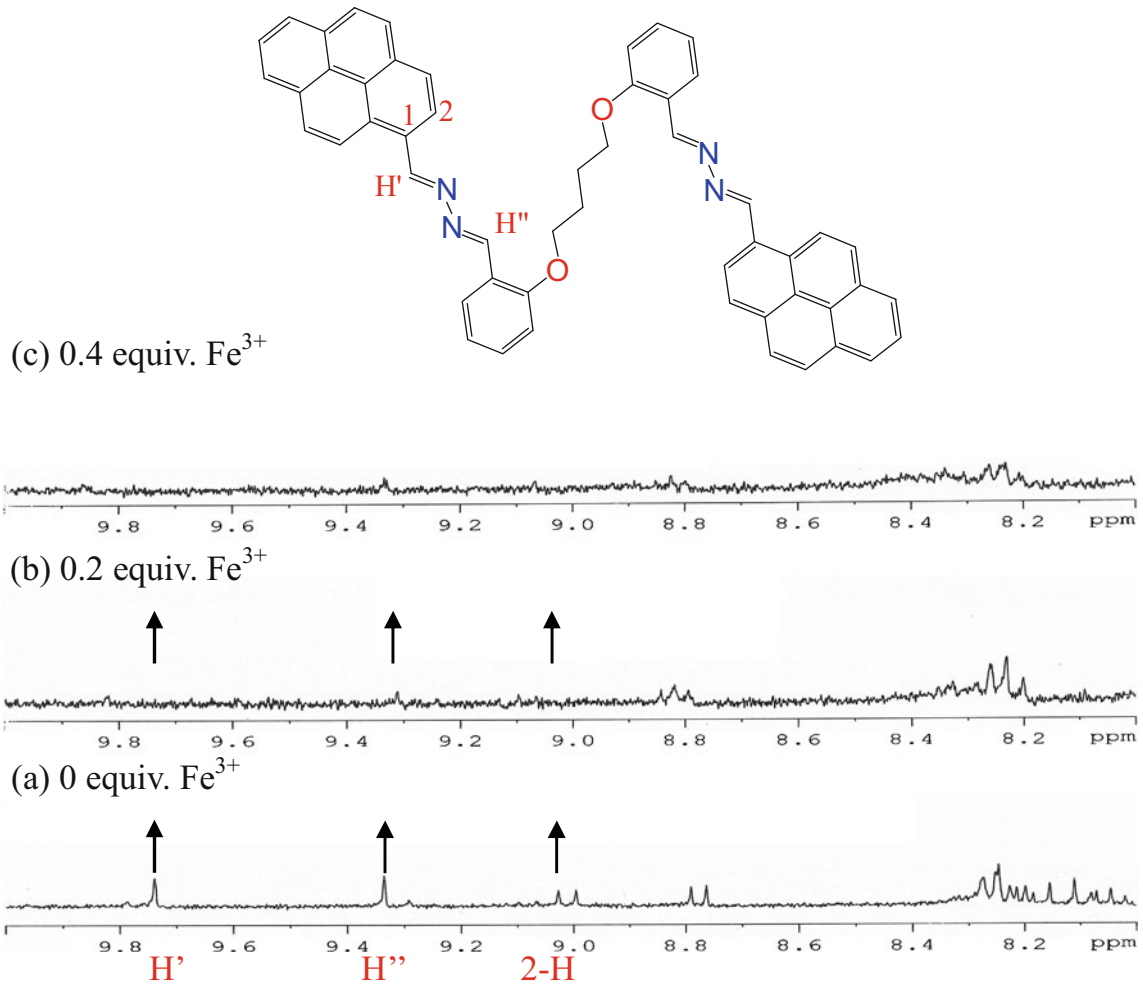


**Fig. 6** $^1H$ NMR (300 MHz) spectra of **1** (2 mM) in the presence of (**a**) 0 equiv, (**b**) 0.2 equiv, (**c**) 0.4 equiv of $Fe^{3+}$ in $CD_3CN/THF\text{-}d_8$ (v/v=1:9)

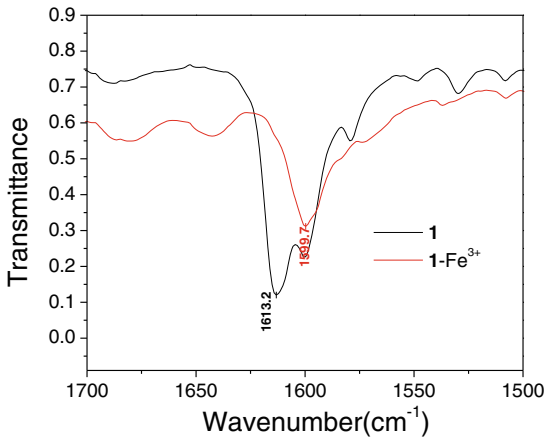


**Fig. 7** IR spectra of **1** and **1**-$Fe^{3+}$ complex

$Fe^{3+}$, $Hg^{2+}$, $K^{+}$, $Mg^{2+}$, $Mn^{2+}$, $Ni^{2+}$, $Pb^{2+}$, and $Zn^{2+}$. $Fe^{3+}$ was the only ion that caused a visible color change (from colorless to yellow) and a green emission from chemosensor **1** (Fig. 1). Figure 2 shows the $Fe^{3+}$ titration with chemosensor **1** monitored by UV–vis and fluorescence spectrometry. After adding $Fe^{3+}$, the maximum absorbance at 382 nm gradually shifted to 363 nm, which is close to the absorption band of pyrene, 335 nm. For fluorescence spectrometry, a new emission band centered at 507 nm formed during the $Fe^{3+}$ titration with chemosensor **1**. After adding 4 equivalents of $Fe^{3+}$, the emission intensity reached a maximum. The quantum yield of the emission band was 0.041, which is 41-fold higher than that of chemosensor **1** at 0.001. The emission band is due to the formation of a pyrene excimer. These observations indicate that $Fe^{3+}$ is the only metal ion that readily binds with chemosensor **1**, causing significant fluorescence enhancement and permitting highly selective detection of $Fe^{3+}$.

In order to understand the binding stoichiometry of **1**-$Fe^{3+}$ complexes, Job plot experiments were carried out. In Fig. 3, the emission intensity at 507 nm is plotted against the molar fraction of chemosensor **1** under a constant total concentration. Maximum emission intensity was reached when the molar fraction was 0.5. These results indicate a 1:1 ratio for **1**-$Fe^{3+}$ complexes, in which one $Fe^{3+}$ ion was bound to one chemosensor **1**. The formation of a 1:1 **1**–$Fe^{3+}$ complex was confirmed by ESI-MS, in which the peak at $m/z$=806.6 indicates a 1:1 stoichiometry for the **1**–$Fe^{3+}$ complex. The association constant $K_a$ was evaluated graphically by plotting $1/\Delta F$ against $1/[Fe^{3+}]$ (Fig. 4). The data was linearly fitted according to the Benesi–Hildebrand equation and the $K_a$ value was obtained from the slope and intercept of the line. The apparent association constant ($K_a$) of $Fe^{3+}$ binding in chemosensor **1** was found to be $1.27\times10^4$ $M^{-1}$.

To study the influence of other metal ions on $Fe^{3+}$ binding with chemosensor **1**, competitive experiments with other metal ions (10 μM) in the presence of $Fe^{3+}$ (10 μM) were performed (Fig. 5). Fluorescence enhancement caused by the mixture of $Fe^{3+}$ with most metal ions was similar to that caused by $Fe^{3+}$ alone. Smaller fluorescence enhancement was observed only when $Fe^{3+}$ was mixed with $Co^{2+}$, $Cu^{2+}$, or $Ni^{2+}$, indicating that $Co^{2+}$, $Cu^{2+}$, and $Ni^{2+}$ compete with $Fe^{3+}$ for binding with chemosensor **1**. None of the other metal ions were found to interfere with the binding of chemosensor **1** with $Fe^{3+}$.

To gain a clearer understanding of the structure of **1**-$Fe^{3+}$ complexes, $^1$H NMR and Infrared (IR) spectroscopy were employed. $Fe^{3+}$ is a paramagnetic ion and can affect the proton signals that are close to the $Fe^{3+}$ binding site. In the $^1$H NMR spectra of chemosensor **1**, the proton (CH=N) signals at 9.57 ppm and 9.24 ppm almost disappeared upon the addition of $Fe^{3+}$ (Fig. 6). These observations indicate the binding of $Fe^{3+}$ with an imine group. The IR spectra were primarily characterized by bands in the double-bond region. Two bands, 1613 $cm^{-1}$ and 1601 $cm^{-1}$, were associated with double bond (C=C and C=N) absorption in chemosensor **1** (Fig. 7). Binding of $Fe^{3+}$ with chemosensor **1** resulted in only one band at 1599 $cm^{-1}$ in the double-bond absorption

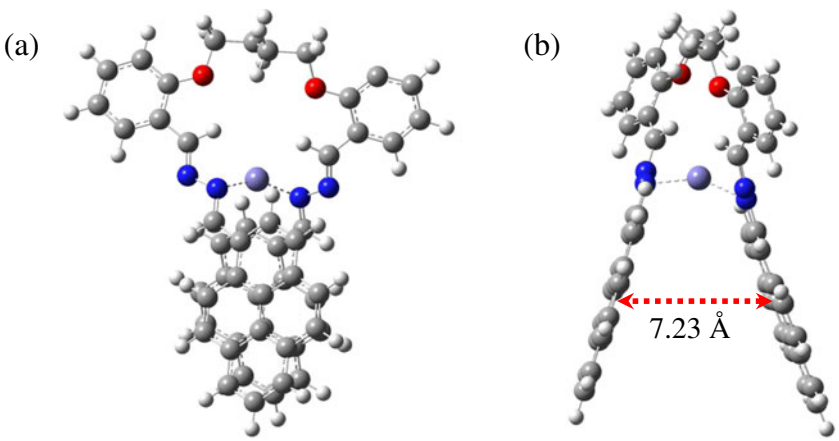


**Fig. 8** Optimized geometries of (**a**) front view and (**b**) side view of the **1**-$Fe^{3+}$ complex calculated with B3LYP/LanL2DZ method. (Blue atom: N, red atom: O, purple atom: Fe)

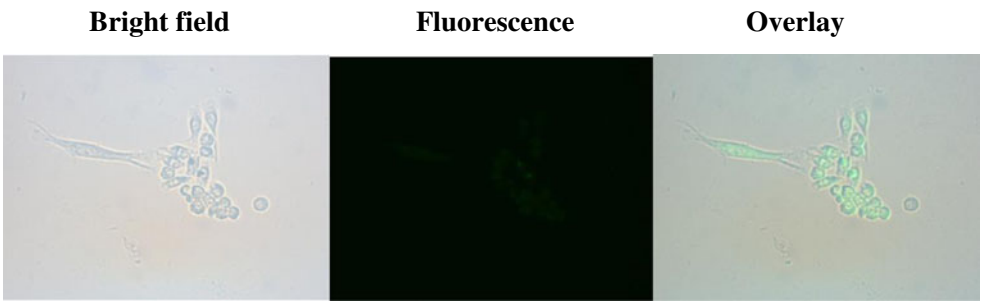


**Fig. 9** $Fe^{3+}$-treated HeLa cell images. (left) Bright field image; (middle) fluorescence image; and (right) merged image

region. This was due to $Fe^{3+}$-binding with **1** through the nitrogen at the imine bonds.

To elucidate the structure of the **1**-$Fe^{3+}$ complex, we employed density functional theory (DFT) calculations using the Gaussian 09 software package. Because of the 1:1 ligand-to-metal ratio of the complexes, as determined from the mass spectrum and Job plot measurements, we applied the B3LYP/LANL2DZ energy optimization routine to determine the possible structure of the **1**-$Fe^{3+}$ complexes. The lowest energy conformation for **1**-$Fe^{3+}$ complexes is shown in Fig. 8. $Fe^{3+}$ binding with chemosensor **1** induced the formation of a Py-Py* excimer. $Fe^{3+}$ is mainly coordinated to two nitrogen atoms at distances of 2.17 Å and 2.17 Å.

Living Cell Imaging

Chemosensor **1** was also applied to living cell imaging. For the detection of $Fe^{3+}$ in living cells, HeLa cells were cultured in DMEM (Dulbecco's Modified Eagle Medium) supplemented with 10 % phosphate-buffered saline (FBS) at 37 °C and 5 % $CO_2$. Cells were plated on 14 mm glass coverslips and allowed to adhere for 24 h. HeLa cells were treated with 10 μM $FeCl_3$ for 30 min and washed with PBS three times. Cells were then incubated with chemosensor **1** (10 μM) for 30 min and washed with PBS to remove the remaining sensor. The images of the HeLa cells were obtained using a fluorescence microscope. Figure 9 shows the images of HeLa cells with chemosensor **1** after the treatment of $Fe^{3+}$. The overlay of fluorescence and bright-field images reveal that the fluorescence signals are localized in the intracellular area, indicating a subcellular distribution of $Fe^{3+}$ and good cell-membrane permeability of chemosensor **1**.

## Conclusion

This study developed a pyrene-based fluorescent chemosensor for $Fe^{3+}$ sensing. The experiment synthesized chemosensor **1** from the reaction of 1-pyrenecarboxaldehyde hydrazone and 1,4-bis(2-formylphenoxy)butane to form two imine bonds between 1,4-bis-phenoxy butane and pyrene. We observed significant fluorescence enhancement with chemosensor **1** in the presence of $Fe^{3+}$. However, adding $Ag^{+}$, $Ca^{2+}$, $Cd^{2+}$, $Co^{2+}$, $Fe^{2+}$, $Hg^{2+}$, $Mg^{2+}$, $Mn^{2+}$, $Ni^{2+}$, $Pb^{2+}$, or $Zn^{2+}$ to the chemosensor solution caused only minimal change in fluorescence emission. This pyrene-based $Fe^{3+}$ chemosensor provides an effective means of sensing $Fe^{3+}$.

**Acknowledgments** We gratefully acknowledge the financial supports of the National Science Council (ROC) and National Chiao Tung University.

## References

1. Cowan JA (1997) Inorganic biochemistry: An introduction. Wiley-VCH, New York, pp 167–255
2. Haas JD, Brownlie T IV (2001) Iron deficiency and reduced work capacity: A critical review of the research to determine a causal relationship. J Nutr 131:676s–688s
3. Burdo JR, Connor JR (2003) Brain iron uptake and homeostatic mechanisms: An overview. BioMetals 16:63–75
4. Bonda DJ, Lee H, Blair JA, Zhu X, Perry G, Smith MA (2011) Role of metal dyshomeostasis in Alzheimer's disease. Metallomics 3:267–270
5. Pithadia AS, Lee MH (2012) Metal-associated amyloid-β species in Alzheimer's disease. Curr Opin Chem Biol 16:67–73
6. Andersen JET (2005) A novel method for the filterless preconcentration of iron. Analyst 130:385–390
7. del Castillo Busto ME, Montes-Bayon M, Blanco-Gonzalez E, Meija J, Sanz-Medel A (2005) Strategies to study human serum transferrin isoforms using integrated liquid chromatography ICPMS, MALDI-TOF, and ESI-Q-TOF detection: Application to chronic alcohol abuse. Anal Chem 77:5615–5621
8. Pomazal K, Prohaska C, Steffan I, Reich G, Huber JFK (1999) Determination of Cu, Fe, Mn, and Zn in blood fractions by SEC-HPLC-ICP-AES coupling. Analyst 124:657–663
9. van den Berg CMG (2006) Chemical speciation of iron in seawater by cathodic stripping voltammetry with dihydroxynaphthalene. Anal Chem 78:156–163
10. Bricks JL, Kovalchuk A, Trieflinger C, Nofz M, Büschel M, Tolmachev AI, Daub J, Rurack K (2005) On the development of sensor molecules that display $Fe^{III}$-amplified fluorescence. J Am Chem Soc 127:13522–13529
11. Xiang Y, Tong A (2006) A new rhodamine-based chemosensor exhibiting selective $Fe^{III}$-amplified fluorescence. Org Lett 8:1549–1552
12. Kennedy DP, Incarvito CD, Burdette SC (2010) FerriCast: A macrocyclic photocage for $Fe^{3+}$. Inorg Chem 49:916–923
13. Zhang L, Zhao J, Zeng X, Mu Mu L, Jiang X, Deng M, Zhang J, Wei G (2011) Tuning with pH: The selectivity of a new rhodamine B derivative chemosensor for $Fe^{3+}$ and $Cu^{2+}$. Sens Actuators B 160:662–669

14. Wang S, Meng X, Zhu M (2011) A naked-eye rhodamine-based fluorescent probe for Fe(III) and its application in living cells. Tetrahedron Lett 52:2840–2843
15. Zhang L, Wang J, Fan J, Guo K, Peng X (2011) A highly selective, fluorescent chemosensor for bioimaging of $Fe^{3+}$. Bioorg Med Chem Lett 21:5413–5416
16. Wei D, Sun Y, Yin J, Wei G, Du Y (2011) Design and application of $Fe^{3+}$ probe for "naked-eye" colorimetric detection in fully aqueous system. Sens Actuators B 160:1316–1321
17. Yang Z, She M, Yin B, Cui J, Zhang Y, Sun W, Li J, Shi Z (2012) Three rhodamine-based "off-on" chemosensors with high selectivity and sensitivity for $Fe^{3+}$ imaging in living cells. J Org Chem 77:1143–1147
18. Kumar M, Kumar R, Bhalla V, Sharma PR, Kaur T, Qurishi Y (2012) Thiacalix[4]arene based fluorescent probe for sensing and imaging of $Fe^{3+}$ ions. Dalton Trans 41:408–412
19. Li Z, Zhang L, Li X, Guo Y, Ni Z, Chen J, Wei L, Yu M (2012) A fluorescent color/intensity changed chemosensor for $Fe^{3+}$ by photo-induced electron transfer (PET) inhibition of fluoranthene derivative. Dyes Pigments 94:60–65
20. Liu S, Wu S (2012) New water-soluble highly selective fluorescent chemosensor for Fe(III) ions and its application to living cell imaging. Sens Actuators B 171–172:1110–1116
21. Thomas F, Serratrice G, Beguin C, Aman ES, Pierre JL, Fontecave M, Laulhere JP (1999) Calcein as a fluorescent probe for ferric iron. J Biol Chem 274:13375–13383
22. Liu JM, Yang JL, Chen CF, Huang ZT (2002) A new fluorescent chemosensor for $Fe^{3+}$ and $Cu^{2+}$ based on calix[4]arene. Tetrahedron Lett 43:9209–9212
23. Ma Y, Luo W, Quinn PJ, Liu Z, Hider RC (2004) Design, synthesis, physicochemical properties, and evaluation of novel iron chelators with fluorescent sensors. J Med Chem 47:6349–6362
24. Tumambac GE, Rosencrance CM, Wolf C (2004) Selective metal ion recognition using a fluorescent 1,8-diquinolylnaphthalene-derived sensor in aqueous solution. Tetrahedron 60:11293–11297
25. Sumner JP, Kopelman R (2005) Alexa Fluor 488 as an iron sensing molecule and its application in PEBBLE nanosensors. Analyst 130:528–533
26. Wu S, Huang Z, Liu S, Chung PK (2012) A pyrene-based highly selective turn-on fluorescent sensor for copper(II) Ion and its application in live cell imaging. J Fluoresc 22:253–259
27. Zhou Z, Cao C, Liu Q, Jiang R (2010) Hybrid orbital deformation (HOD) effect and spectral Red-shift property of nonplanar porphyrin. Org Lett 12:1780–1783
28. Senthilvelan A, Ho I, Chang K, Lee G, Liu Y, Chung W (2009) Cooperative recognition of a copper cation and anion by a calix[4]arene substituted at the lower rim by a β-amino-α, β-unsaturated ketone. Chem Eur J 15:6152–6160
29. Benesi HA, Hildebrand JH (1949) A spectrophotometric investigation of the interaction of iodine with aromatic hydrocarbons. J Am Chem Soc 71:2703–2707
30. Wu S, Wang T, Liu S (2010) A highly selective turn-on fluorescent chemosensor for copper(II) ion. Tetrahedron 66:9655–9658
31. Maeda H, Inoue Y, Ishida H, Mizuno K (2001) UV absorption and fluorescence properties of pyrene derivatives having trimethylsilyl, trimethylgermyl, and trimethylstannyl groups. Chem Lett 1224–1225
32. Karpovich DS, Blanchard GJ (1995) Relating the polaritydependent fluorescence response of pyrene to vibronic coupling. Achieving a fundamental understanding of the py polarity scale. J Phys Chem 99:3951–3958